Power Allocation for Indoor Distributed Antenna System Based on Path Loss Prediction at 6 GHz

Liang Xin†, Jianhua Zhang*, Xiaofan Li
Key Laboratory of Universal Wireless Communications, Ministry of Education
Wireless Technology Innovation Institute (WTI), Beijing University of Posts and Telecommunications
Beijing 100876, China
Email:†xinliang.jia@163.com, *jhzhang@bupt.edu.cn

***Abstract*—Due to the difficulty in obtaining the perfect channel state information (CSI), in this paper, the power allocation algorithm is investigated with only large scale information. Based on the measured channel data at 6 GHz, log-distance (LGD) model and linear-distance (LID) model are used to predict the large scale information or path loss (PL) firstly, and both achieve a good prediction precision. Then water-filling algorithm with the predicted PL (WPP) is proposed in this paper for frequency selective fading channel. The proposed algorithm can lead to a 33% increase in average capacity compared with uniform power allocation (UPA) scheme, and outperform the selective transmission (ST) scheme, especially in high transmitted signal to noise ratio (SNR). Besides, the robustness of the proposed algorithm is evaluated, which depends on the difference of PLs among radio links.**

I. Introduction

With the increasing demands for high speed data-rates transmission in indoor environment, some indoor enhanced technologies have attracted lots of attentions [1, 2]. Distributed antenna system (DAS), as a promising technique, has been extensively studied in [1, 3]. In DAS, transmit antenna units (TAUs) are geographically separated, and connected to the central unit (CU) via wires or fibers with low power loss. Thus, DAS can reduce access distance, to achieve a good power coverage and system capacity [1].

Since the power allocation scheme is significant on improving system capacity, the allocation algorithm should be designed, to achieve the capacity of DAS. Without the priori channel state information (CSI), the uniform power allocation (UPA) is the optimal scheme [2], in which all subchannels are fed with the same power. Unfortunately, it can not exploit the capacity potential of DAS. When the perfect CSI is known at CU, the water-filling power allocation algorithm based on eigenvalues of channel matrix can achieve the maximum data rate [2]. However, the perfect channel information is usually difficult to obtain. Especially when user equipments (UEs) or surrounding scatters are in movement, the channel parameters are time-variant. The imperfect CSI may bring about the degradation of performance of the water-filling algorithm on channel eigenvalues.

Typically, the perfect CSI consists of large scale CSI (i.e. large scale fading) and small scale CSI (i.e. small scale fading) [3]. Rapid change for small scale fading results in difficulty in estimation or prediction [3] at the receiver (RX), but the large scale fading, which changes mildly over time or distance [4], can be obtained more easily. In order to make use of it, some algorithms are proposed in [3, 5]. In [5], perfect large scale fading information is assumed to be known at the CU, and a power allocation algorithm is proposed under the total power constraint. However, the proposed algorithm is just for the flat-fading quasi-static model, which is not applicable to frequency selective fading channel directly. Besides, when the large scale CSI is imperfect, the performance of the proposed algorithms in [3, 5] should be evaluated.

Motivated by the analysis above, our research is as follows:

- Based on wideband channel measurement at 6 GHz, the log-distance (LGD) model and linear-distance (LID) model are adopted to predict the large scale fading or path loss (PL), different from the methodology adopted in [3, 5], which is based on assumed large scale CSI.
- A water-filling algorithm based on predicted PL (WPP) is proposed for frequency selective fading channel. Its capacity performance and robustness are evaluated.

The rest of the paper is organized as follows. Section II presents PL prediction models, and the power allocation algorithms is proposed in Section III. Section IV describes measurement equipment and environment. Performance of the proposed algorithm is analyzed in Section V. Section VI concludes the paper.

II. PL Prediction Models for DAS

We consider a DAS with M geographically distributed TAUs, and a UE with N receive antennas. $\mathbf{H}(t, f_k)$ is the $N \times M$ channel matrix at time t and the f_k^{th} $(k = 1, \ldots, K)$ subcarrier frequency, which encompasses small scale fading and large scale fading [3],

$$\mathbf{H}(t, f_k) = \mathbf{S}(f_k)\boldsymbol{\zeta}(f_k) \tag{1}$$

where $\mathbf{S}(f_k)$ is the small scale fading, representing the rapid variation of received power over a short distance or time, which can hardly be predicted precisely. The symbol $\boldsymbol{\zeta}(f_k)$ indicates the large scale fading denoting average attenuation in the local area [6], and $\boldsymbol{\zeta}(f_k) = \mathrm{diag}\left(\zeta_1(f_k), \ldots, \zeta_m(f_k), \ldots, \zeta_M(f_k)\right)$, where $\zeta_m(f_k)$ is a constant in the local area. When the system bandwidth is far smaller

than the center frequency, $\boldsymbol{\zeta} \approx \boldsymbol{\zeta}(f_k)\,(k = 1, \ldots, K)$ [7]. Besides, the elements in $\boldsymbol{\zeta}$ satisfy

$$\zeta_i^2 = 10^{-PL_i/10}; i = 1, \ldots, M. \tag{2}$$

where PL_i is the perfect PL between the UE and the i^{th} TAU. From the same TAU, the PLs of the multiple receive antennas are similar.

Since the large scale fading changes mildly, it is easy to be obtained by predicting PL with the LGD and LID model etc.

1) LGD Model: LGD model is widely used for indoor scenario and outdoor scenario [4], and expressed as

$$\hat{PL}_i(d) = A + n \cdot 10\log_{10}(d) \tag{3}$$

where d is the distance between the transmitter (TX) and RX. $\hat{PL}_i(d)$ is the predicted PL between the UE and the i^{th} TAU. A indicates the PL intercept, and n is the PL exponent representing the rate at which PL increases with distance. In free space (FS) scenario, n equals 2, where the received signal has only line of sight (LOS) path, without reflected and scattered multipath components. For other radio scenarios, A and n vary, and can be estimated according to measured channel data.

2) LID Model: LID model is proposed by Devasirvatham in [8] based on the measurements for indoor scenario at 850 MHz, 1.7 GHz, and 4.0 GHz. The LID model is written as

$$\hat{PL}_i(d) = PL_{FS} + \alpha \cdot d = 32.4 + 20\log_{10}(f_c \cdot d) + \alpha \cdot d \tag{4}$$

where α is an attenuation constant in dB/m. The LID model includes two parts: one is the free space loss PL_{FS} ($PL_{FS} = 32.4 + 20\log_{10}(f_c \cdot d)$, where f_c is the carrier frequency); the other is the additional attenuation caused by the obstruction between TX and RX.

In order to better fit our measured data, a parameter β is introduced, thus the LID model is rewritten as:

$$\hat{PL}_i(d) = PL_{FS} + \alpha \cdot d + \beta = B + 20\log_{10}(d) + \alpha \cdot d \tag{5}$$

where $B = 32.4 + 20\log_{10}(f_c) + \beta$.

With the interference of shadow fading [4], both models can not provide perfect prediction. The error exists between the perfect PL and the predicted PL, which is treated as a random variable X_σ, with the standard deviation of σ indicating the prediction precision,

$$PL_i = \hat{PL}_i(d) + X_\sigma; i = 1, \ldots, M. \tag{6}$$

Thus, the obtained large scale fading matrix $\hat{\boldsymbol{\zeta}}$ satisfies

$$\hat{\zeta}_i^2 = 10^{-\hat{PL}_i(d)/10}; i = 1, \ldots, M. \tag{7}$$

where $\hat{\zeta}_i$ is the element in $\hat{\boldsymbol{\zeta}}$.

III. Power Allocation Algorithm for DAS

In the DAS illustrated in Section II, $\mathbf{Q}(f_k)$ is normalized $N \times M$ transmit covariance matrix of subcarrier f_k, and $\rho(f_k)$ denotes signal-to-noise ratio (SNR) which is the quotient between signal power fed into M transmit antennas and average noise power in a transmit antenna at the f_k^{th} subcarrier. For a frequency selective fading channel, the mutual information I is obtained by [9]

$$I = \frac{1}{K}\sum_{k=1}^{K}\log_2\det\left(\mathbf{I}_N + \rho(f_k)\mathbf{H}(t, f_k)\mathbf{Q}(f_k)\mathbf{H}^H(t, f_k)\right) \tag{8}$$

where $(\cdot)^H$ means the conjugate transposition.

The maximum mutual information can be achieved when the perfect CSI is known, and the transmit covariance matrix $\mathbf{Q}(f_k)$ is optimized with a water-filling algorithm [2, 9] based on channel eigenvalues. Unfortunately, the difficulty in obtaining small scale fading makes the perfect CSI unavailable, which would degrade the performance of the water-filling algorithm. Nevertheless, the large scale fading can be predicted easily, power allocation algorithm with large scale CSI is investigated in this paper.

With the predicted large scale CSI $\hat{\boldsymbol{\zeta}}$, it still needs complex numerical optimization to get the optimal $\mathbf{Q}(f_k)$ in (8). In order to reduce the complexity, the average mutual information ($\mathrm{E}\left[\hat{I}\right]$) in a local area is introduced, and we turn to optimize the upper bound of ($\mathrm{E}\left[\hat{I}\right]$).

In this work, the elements in $\mathbf{S}(f_k)$ are assumed as independent and identically distributed (i.i.d) complex Gaussian variables with zero mean and unit variance, and all the subcarriers are fed with the same transmitted power. That is, $\forall k, \mathbf{Q} = \mathbf{Q}(f_k)$ and $\rho = \rho(f_k)$. Besides, $\mathbf{Q}$ is assumed as a diagonal matrix, i.e. $\mathbf{Q} = \mathrm{diag}(q_1, \ldots, q_i, \ldots, q_M)$, where q_i is the power fed into the i^{th} TAU, which would provide the maximum average mutual information demonstrated in [5]. Thus the upper bound of $\mathrm{E}\left[\hat{I}\right]$ is derived as

$$\begin{aligned}
\mathrm{E}\left[\hat{I}\right] &= \mathrm{E}\left[\frac{1}{K}\sum_{k=1}^{K}\log_2\det\left(\mathbf{I}_N + \rho\hat{\mathbf{H}}(t, f_k)\mathbf{Q}\hat{\mathbf{H}}^H(t, f_k)\right)\right] \\
&= \mathrm{E}\left[\frac{1}{K}\sum_{k=1}^{K}\log_2\det\left(\mathbf{I}_M + \rho\hat{\mathbf{H}}^H(t, f_k)\,\hat{\mathbf{H}}(t, f_k)\,\mathbf{Q}\right)\right] \\
&\le \frac{1}{K}\sum_{k=1}^{K}\log_2\det\left(\mathbf{I}_M + \rho\mathrm{E}\left[\hat{\mathbf{H}}^H(t, f_k)\,\hat{\mathbf{H}}(t, f_k)\right]\mathbf{Q}\right) \\
&= \frac{1}{K}\sum_{k=1}^{K}\log_2\det\left(\mathbf{I}_M + \rho\hat{\boldsymbol{\zeta}}^H\mathrm{E}\left[\mathbf{S}^H(f_k)\mathbf{S}(f_k)\right]\hat{\boldsymbol{\zeta}}\mathbf{Q}\right) \\
&= \log_2\det\left(\mathbf{I}_M + N\rho\hat{\boldsymbol{\zeta}}^H\hat{\boldsymbol{\zeta}}\mathbf{Q}\right) = \sum_{i=1}^{M}\log_2\left(1 + N\rho\hat{\zeta}_i^2 q_i\right)
\end{aligned} \tag{9}$$

where $\hat{\mathbf{H}}(t, f_k) = \mathbf{S}(f_k)\hat{\boldsymbol{\zeta}}$. The second quality in (9) follows from the identical equation that $\det(\mathbf{I}_M + \mathbf{XY}) = \det(\mathbf{I}_N + \mathbf{YX})$, where $\mathbf{X}$ is the $M \times N$ matrix and $\mathbf{Y}$ is the $N \times M$ matrix, and the first inequality draws from the property that $\mathrm{E}[\log(\cdot)] \le \log(\mathrm{E}[\cdot])$, since $\log(\cdot)$ is a concave function [5].

In order to maximize the upper bound in (9), a water-filling algorithm [2, 9] based on predicted PL (WPP) is adopted. The optimal power allocation is attained by

$$q_i = \begin{cases} \mu - \frac{1}{N\rho\hat{\zeta}_i^2} = \mu - \frac{10^{\hat{PL}_i(d)/10}}{N\rho}; \mu > \frac{10^{\hat{PL}_i(d)/10}}{N\rho} \\ 0 \qquad\qquad\qquad\qquad\quad ; \text{or else} \end{cases} ; i = 1, \ldots, M. \tag{10}$$

where q_i is determined according to the total power constraint of $\sum_{i=1}^{M} q_i = 1$.

With the $\mathbf{Q}$ determined in (10), the achievable data rate is obtained through substituting $\mathbf{Q}$ into (8).

Besides, when prediction error is zero (that is $X_\sigma = 0$), the (10) is referred as water-filling with the perfect PL (WPE), which is difficult to be achieved.

IV. Measurement Equipment and Environment

Aiming at evaluating the performance and robustness of the proposed power allocation algorithm, a channel measurement has been performed in Beijing University of Posts and Telecommunications (BUPT), China, with Elektrobit Propsound channel sounder. Two stable rubidium frequency references are used for accurate synchronization between TX and RX. Before the measurement, a back-to-back test is conducted to obtain the system response for calibration purpose. The measurement system parameters are detailed in Table I.

TABLE I
Measurement System Parameters

Parameter	Value
Center Frequency [GHz]	6
Bandwidth [MHz]	100
Transmitted Power [dBm]	24
Hight of TAUs/RX [m]	2.7/2
PN Code Length [chips]	255

The measurement campaign is conducted at the first floor shown in Fig. 1 inside a 7-floor teaching building with the dimension of 120 m × 45 m × 6 m for each. The 3 TAUs, denoted as TX1 ~ TX3, are geographically separated, and each is equipped with single vertical-polarized dipole (VPD). They transmit the same pseudo-random (PN) code sequence of length 255 with a chip rate of 100 MHz in a time-division multiplexing (TDM) mode within a channel coherence time. Channel impulse responses (CIRs) are collected at RX with single VPD, by a sliding correlator which correlates the received signal with a synchronized copy of the transmitted PN code sequence. With the Fourier transformation, channel frequency response can be obtained from measured CIRs. During the measurement, RX can move along routes denoted as route 1 ~ route 13 at the speed of 1-2 m/s. Since a burst model [10] is adopted during the channel measurement, where there is a break after transmitting 4 cycles. Therefore, the continuously measured 4 cycles at RX can be considered to be from 4 virtual receive antennas.

V. Results and Analysis

Since the channel sounder is operated in the burst mode, the UE is considered to employ 4 virtual receive antennas. Thus, the measurement system can be equivalent to a DAS with 3 TAUs and a UE with 4 antennas. Before applying the proposed algorithm described in Section III, the PL is predicted by LGD and LID model firstly.

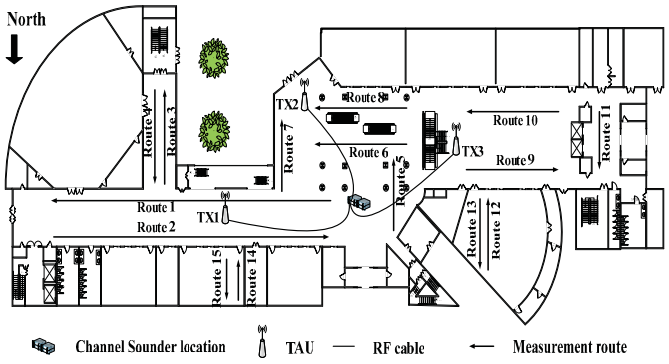

Fig. 1. The skeleton map of measurement scenario in BUPT for indoor DAS.

A. PL Prediction for DAS

In Fig. 1, we just consider the corridor scenario e.g. route 1 ~ 2. When RX moves on the corridor, for TX1, it is LOS propagation without obstruction. The propagation signals from TX2 may be partly obstructed by the pillars or concreted walls, which is categorized as obstructed LOS (OLOS) propagation. For TX3, it is non-LOS (NLOS) propagation, because the signals would be completely obstructed by concrete walls.

Seen from Fig. 2, the PLs at 6 GHz in LOS case are better than FS. In OLOS case, the propagation signals are partially obstructed. Thus, at some locations where LOS propagation is dominating, the PLs are better than FS; at others, the signals may experience more attenuation than FS due to obstruction by walls or pillars. Finally for NLOS case, received signals are greatly attenuated with the worst PLs. At d = 20 m, PL in NLOS case is 20 dB worse than that in LOS case, 13.1 dB worse when compared to OLOS case. Among the three propagation scenarios, the different transmission mechanisms result in significant difference in PLs. Therefore, they should be modeled, respectively. From Fig. 2, PLs for these cases are well fitted by LGD and LID model.

TABLE II
Model Parameters in LOS, OLOS and NLOS Case

Case	PL Prediction Model [in dB]
LGD Model	
LOS	$\hat{PL}_1(d) = 45.4 + 17.0 \cdot \log_{10}(d)$
OLOS	$\hat{PL}_2(d) = 18.1 + 44.6 \cdot \log_{10}(d)$
NLOS	$\hat{PL}_3(d) = 44.6 + 33.1 \cdot \log_{10}(d)$
LID Model	
LOS	$\hat{PL}_1(d) = 28.3 + 20\log_{10}(d) - 0.12 \cdot d$
OLOS	$\hat{PL}_2(d) = 25.5 + 20\log_{10}(d) + 0.43 \cdot d$
NLOS	$\hat{PL}_3(d) = 44.3 + 20\log_{10}(d) + 0.14 \cdot d$

where $\hat{PL}_i(d)$ is the predicted PL between the UE and TXi.

In Table II, the PL exponent in LGD model for LOS case is smaller than the FS exponent 2. It is reasonable that in an enclosed indoor scenario, the received signals are the summation of many multipath components. In addition to LOS component, other components reflected by floors, walls and other objects, may be powerful enough, which also results in

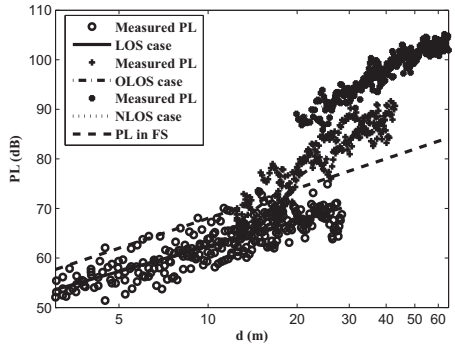

(a) LGD model

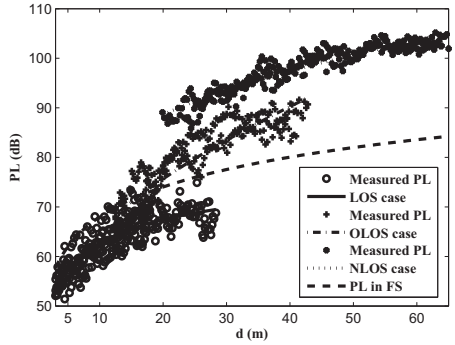

(b) LID model

Fig. 2. PLs and prediction models in LOS, OLOS and NLOS case.

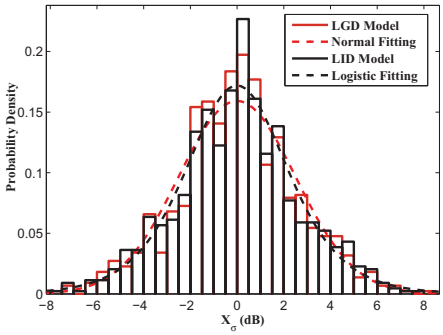

Fig. 3. PDFs of X_σ in LDG and LID prediction model.

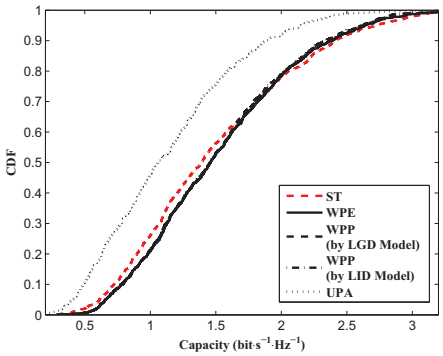

Fig. 4. CDFs of capacity at transmitted SNR=80 dB.

a negative attenuation constant α in LID model. The similar results are observed in [11], where the PL exponents for an indoor office environment at 2.4 GHz, 4.75 GHz and 11.5 GHz are all smaller than 2 in LOS case. For OLOS and NLOS case, the PL exponents are higher than 2, representing that PL changes rapidly with distance. The attenuation constants in OLOS and NLOS case are greater than 0, which indicates that additional attenuation caused by obstruction increases linearly with the distance.

In order to evaluate the prediction precision, the standard deviation of X_σ is calculated. The prediction errors in LOS, OLOS and NLOS cases are considered together. The standard deviations of X_σ for LGD and LID model are around 2.5, reflecting a good prediction achieved by both models. Beside, the probability density functions (PDFs) of X_σ for both models are presented in Fig. 3, respectively.

With the chi-square test at the level of significance of 0.05, the predicted error of LGD model obeys normal distribution with zero mean and standard deviation of 2.5. While for LIG prediction model, the PDF of X_σ is similar to the logistic distribution with mean value of -0.004 and standard deviation of 2.64. Thus, the statistic characteristic of X_σ depends on the PL prediction model chosen.

B. Power Allocation Based on Predicted PL

1) Capacity Evaluation: When transmitted SNR is 80 dB, the average allocated power for every port is shown in Table III under different allocation schemes, and cumulative density functions (CDFs) of capacity are presented in Fig. 4.

TABLE III
THE AVERAGE ALLOCATED POWER AT TRANSMITTED SNR=80 DB

Power Allocation Schemes	TX1	TX2	TX3
UPA	1/3	1/3	1/3
ST	1	0	0
WPE	0.75	0.25	0
WPP by LGD Model	0.74	0.26	0
WPP by LID Model	0.74	0.26	0

Where ST is selective transmission where only one TAU is chosen with smallest predicted PL every time.

The WPE scheme and WPP scheme by both prediction models enjoy almost the same average power allocation for 3 ports in Table III, which contributes to their proximate capacity, shown in Fig. 4. Besides, in the UPA scheme, 3 TAUs are fed with equal power. While in the WPP scheme, the power is distributed into the two TAUs with the smallest PL. Thus, the WPP scheme by both models outperforms the UPA scheme, and brings about a 33% increase in average capacity. For the ST scheme, only one TAU is selected, which just can provide one independent data stream on a vector channel. But in the WPP scheme, a matrix channel can be created to provide

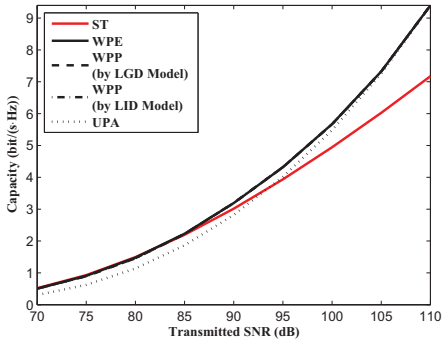

Fig. 5. Ergodic capacity at different transmitted SNRs.

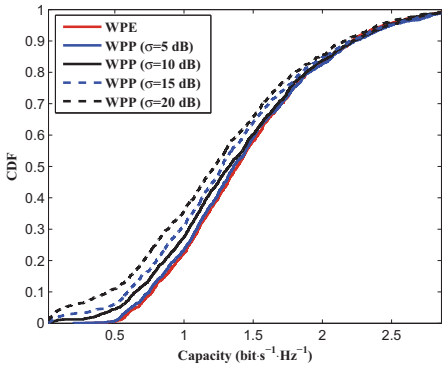

Fig. 6. The performance of the WPP algorithm under different prediction precisions.

multiple independent data streams simultaneously [2, 9]. So the performance of the WPP scheme is better than the ST scheme, and advantage of the WPP scheme is obvious at high transmitted SNR, shown in Fig. 5. In addition, the complexity of the WPP algorithm is just related to the number of TAUs. Therefore, the proposed algorithm is very practical.

However, when the transmitted SNR is very high ($\geq$ 105 dB), the power is sufficient to make sure all the subchannels have a good quality. Thus, more antennas are excited for data transmission, and the advantage of the WPP algorithm shrinks compared with the UPA scheme.

2) Effect of Prediction Error: In order to evaluate the robustness of the proposed algorithm, the performance under different prediction precisions is analyzed. We assume the prediction error X_σ is a zero-mean Gaussian random variable, and $\hat{PL}_i(d)$ is not calculated by the PL models as before but from $\hat{PL}_i(d) = PL_i - X_\sigma; (i = 1, 2, 3)$, where PL_i is the perfect PL obtained from channel measurement. At transmitted SNR=80 dB, the CDFs of capacity at different standard deviations are presented in Fig. 6. When $\sigma < 10$ dB, the WPP scheme has a good robustness with the interference of prediction error, whose effect on performance of the WPP scheme is negligible. However, at $\sigma \geq 10$ dB, performance of the WPP algorithm begins to deteriorate.

At transmitted SNR=80 dB, only TX1 and TX2 are fed with power seen in Table III. In addition, from Fig. 3, PL for TX1 is about 10 dB better than that for TX2 in average. Therefore, a small σ ($\sigma < 10$ dB) has weak effect on the power allocation for two antennas, resulting in insensibility of the WPP algorithm to prediction error. However, if $\sigma \geq 10$ dB, the impact of prediction error on allocated powers into two antennas is significant, giving rise to degradation of its performance.

VI. Conclusions

In this paper, the power allocation algorithm is studied for DAS with large scale information. The proposed water-filling algorithm based on predicted PL by LGD and LID model can introduce a 33% increase in capacity compared with the UPA scheme, and have better performance than the ST scheme, especially at high transmitted SNR. Further more, the difference in PLs among the radio links has great influence on robustness of the proposed algorithm. When the difference in PLs is significant, the performance of the proposed algorithm is not sensitive to prediction precision.

Acknowledgments

This research is supported by China Information Technology Designing & Consulting Institute Ltd (CITC)-School of Information and Communication Engineering (SICE) in BUPT Graduate Innovation Fund for 2011, and National Technology Supported Plan Grant 2012BAF14B01.

References

[1] D. Castanheira and A. Gameiro, "Distributed antenna system capacity scaling [coordinated and distributed mimo]," *IEEE Wireless Communication Magazine*, vol. 17, no. 3, pp. 68-75, 2010.

[2] D. Gesbert, M. Shafi, S. Da-shan, P. Smith, and A. Naguib, "From theory to practice: an overview of MIMO space-time coded wireless systems," *IEEE Journal on Selected Areas in Communications*, vol.21, no.3, pp. 281-302, April 2003.

[3] W. Feng, Y. Li, S. Zhou, and J. Wang, "Downlink power allocation for distributed antenna systems in a multi-cell environment," *the 5th International Conference on Wireless Communications, Networking and Mobile Computing*, pp.1-4, Septepber 2009.

[4] A. Molisch, L. Greenstein, and M. Shafi, "Propagation issues for cognitive radio," *Proceedings of the IEEE*, vol.97, no.5, pp.787-804, May 2009.

[5] H. Zhuang, L Dai, L. Xiao, and Y. Yao, "Spectral efficiency of distributed antenna system with random antenna layout," *Electronics Letters*, vol.39, no.6, pp. 495- 496, March 2003.

[6] J. Salo, L. Vuokko, H. El-Sallabi, and P. Vainikainen, "An additive model as a physical basis for shadow fading," IEEE Transactions on Vehicular Technology, vol.56, no.1, pp.13-26, January 2007.

[7] A. Alvarez, G. Valera, M. Lobeira, R. Torres, and J. Garcia, "New channel impulse response model for uwb indoor system simulations," *in Proceedings of IEEE Vehicular Technology Conference*, pp. 1-5, 2003.

[8] D. Devasirvatham, C. Banerjee, M. Krain, and D. Rappaport,"Multi-frequency radiowave propagation measurements in the portable radio environment," *IEEE International Conference on Communications*, pp.1334-1340 vol.4, April 1990.

[9] A. Paulraj, R. Nabar, and D. Gore, *Introduction to Space-Time Wireless Communications*. London, UK: Cambridge University Press, 2003.

[10] N. Czink, E. Bonek, and J. Ylitalo, "The interdependence of cluster parameters in mimo channel modeling," *in Proceedings of the 1st European Conference on Antennas and Propagation (EuCAP '06)*, pp. 1C6, Nice, France, 2006.

[11] G. Janssen, P. Stigter and R. Prasad, "Wideband indoor channel measurements and BER analysis of frequency selective multipath channels at 2.4 GHz, 4.75 GHz and 11.5 GHz," *IEEE Transactions on Vehicular Technology*, vol. 44, no. 10, pp. 1272-1288, 1996.